

# COOKIE-CUTTER HALOS: THE REMARKABLE CONSTANCY OF THE STELLAR MASS FUNCTION OF SATELLITE GALAXIES AT $0.2 < z < 1.2$

TOMER TAL<sup>1,6</sup>, RYAN F. QUADRI<sup>2</sup>, ADAM MUZZIN<sup>3</sup>, DANILO MARCHESINI<sup>4</sup>, AND MAURO STEFANON<sup>5</sup>

<sup>1</sup>UCO/Lick Observatory, University of California, Santa Cruz, CA 95064, USA; [tal@ucolick.org](mailto:tal@ucolick.org)

<sup>2</sup>Department of Physics and Astronomy, Texas A&M University, College Station, TX 77843, USA

<sup>3</sup>Leiden Observatory, Leiden University, NL-2300 RA Leiden, The Netherlands

<sup>4</sup>Department of Physics and Astronomy, Tufts University, Medford, MA 02155, USA

<sup>5</sup>Department of Physics and Astronomy, University of Missouri, Columbia MO, 65211, USA

*Submitted to ApJ Letters*

## ABSTRACT

We present an observational study of the stellar mass function of satellite galaxies around central galaxies at  $0.2 < z < 1.2$ . Using statistical background subtraction of contaminating sources we derive satellite stellar mass distributions in four bins of central galaxy mass in three redshift ranges. Our results show that the stellar mass function of satellite galaxies increases with central galaxy mass, and that the distribution of satellite masses at fixed central mass is at most weakly dependent on redshift. We conclude that the average mass distribution of galaxies in groups is remarkably universal even out to  $z = 1.2$  and that it can be uniquely characterized by the group central galaxy mass. This further suggests that as central galaxies grow in stellar mass, they do so in tandem with the mass growth of their satellites. Finally, we classify all galaxies as either star forming or quiescent, and derive the mass functions of each subpopulation separately. We find that the mass distribution of both star forming and quiescent satellites show minimal redshift dependence at fixed central mass. However, while the fraction of quiescent satellite galaxies increases rapidly with increasing central galaxy mass, that of star forming satellites decreases.

**Keywords:** galaxies: groups: general – galaxies: luminosity function, mass function

## 1. INTRODUCTION

Galaxy mass distributions in the universe have long been regarded as an important characteristic of galaxy populations, and as a key tracer of their evolution over time. Many of the physical processes that govern the evolution of galaxies directly affect their masses, and as a consequence, also their global number density. Galaxy mergers, star formation and feedback mechanisms all leave their imprint on the shape and normalization of the galaxy stellar mass function. Therefore, tremendous effort has been devoted to observational studies of the global distribution of galaxy masses, pushing this measurement to higher redshifts and to lower mass limits (e.g., Bell et al. 2003; Bundy et al. 2006; Marchesini et al. 2009; Ilbert et al. 2010; Muzzin et al. 2013a; Tomczak et al. 2014). Similarly, the success of many numerical investigations of galaxy evolution is determined in large part by their ability to reproduce the observed galaxy stellar mass function (e.g., Croton et al. 2006; Guo et al. 2011).

Galaxies that reside in groups and clusters are subject to environmental processes that affect their star formation rates and masses. Consequently, the distribution of galaxy masses in such halos is somewhat different from the overall stellar mass function. It is characterized by a gap between the mass (or luminosity) of central galaxies and their satellite galaxies and it exhibits different fractions of star forming and quiescent galaxies in different environments (e.g., Jones et al. 2003; Milosavljević et al. 2006; van den Bosch et al. 2007; Bolzonella et al. 2010; Kovač et al. 2010; Vulcani et al. 2013; Knobel et al. 2013; Deason et al. 2013; Van der Burg 2013). In a series of papers, Yang et al. analyzed group membership

catalogs using extensive photometric and spectroscopic data from the Sloan Digital Sky Survey, to analyze the mass distribution of galaxies in groups at  $z \sim 0$ . They found that the distribution of satellite galaxy masses can be reliably predicted from the halo mass of a given group, or alternatively, from the stellar mass of its central galaxy (the conditional stellar mass function; Yang et al. 2007, 2008, 2009).

In this letter we follow an alternative approach to study the stellar mass function of galaxies in groups in a large range of satellite and central masses, and over a significant redshift range. Instead of assigning membership of individual galaxies to specific halos, we measure the average masses of galaxies in these environments using statistical background subtraction of contaminating sources. This technique has been shown to be effective in studies of satellite galaxies in general (e.g., Masjedi et al. 2006, 2008; Tal et al. 2012a, 2013; Budzynski et al. 2012; Nierenberg et al. 2012), and of the stellar mass function of satellites in particular (e.g., Tal & van Dokkum 2011; Tal et al. 2012b; Wang & White 2012). One of the main advantages to this approach is that it allows us to rely on photometric surveys and thus probe the intermediate redshift universe using mass limited samples.

Throughout the letter we adopt the following cosmological parameters:  $\Omega_m = 0.3$ ,  $\Omega_\Lambda = 0.7$  and  $H_0 = 70$  km s<sup>-1</sup> Mpc<sup>-1</sup>.

## 2. PHOTOMETRIC CATALOG AND SAMPLE SELECTION

Galaxies for this study were selected from the public photometric catalog<sup>1</sup> of Muzzin et al. (2013b), based on the first data release of UltraVISTA, an ongoing ultra deep near-infrared survey with the European South-

<sup>6</sup> NSF Astronomy and Astrophysics Postdoctoral Fellow

<sup>1</sup> [www.strw.leidenuniv.nl/galaxyevolution/ULTRAVISTA](http://www.strw.leidenuniv.nl/galaxyevolution/ULTRAVISTA)

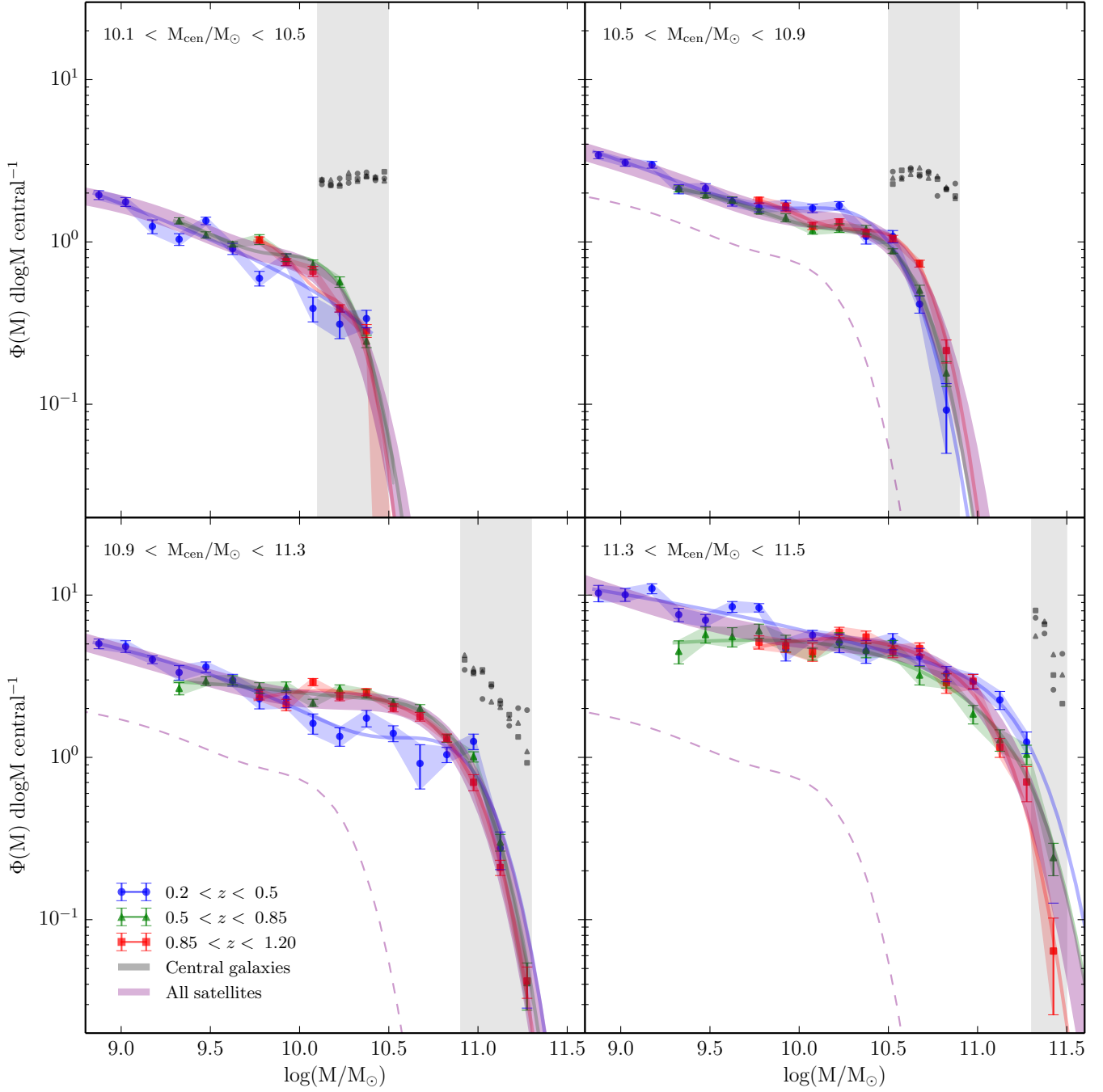


**Figure 1.** Redshift dependence of the satellite stellar mass function at  $0.2 < z < 1.2$  in four bins of fixed central galaxy mass. Black points and gray regions show the range of central galaxy masses in each panel. Blue, green and red points represent satellite masses at different redshifts, as well as their corresponding statistical uncertainties. Blue, green and red lines are double-Schechter fits to the data at each redshift and thick purple lines are fits to the entire satellite population in each panel. The stellar mass functions of satellite galaxies at a given central galaxy mass are consistent with one another across the studied redshift range over essentially the entire spectrum of analyzed satellite masses. In contrast, the distribution of satellite masses varies significantly with the mass of their central galaxy, in agreement with the conditional stellar mass function model (Yang et al. 2009). This weak dependence on redshift, and strong dependence on central mass imply that the average mass distribution of satellite galaxies can be reliably predicted solely from the mass of their central at  $0.2 < z < 1.2$ .

ern Observatory VISTA survey telescope (McCracken et al. 2012). The catalog covers an area of  $1.62 \text{ deg}^2$  in the COSMOS field, includes photometry in 30 bands, and provides excellent photometric redshifts ( $\sigma_z/(1+z) = 0.013$  with catastrophic outlier fraction of 1.56%). Galaxy stellar masses are calculated assuming Kroupa (2001) initial mass function, and are estimated to be 95% complete down to a stellar mass limit of  $5 \times 10^9 M_\odot$  at  $z < 1.2$  (Muzzin et al. 2013a).

### 2.1. Central Galaxy Identification

We identified central galaxy candidates from the UltraVISTA catalog in three stellar mass bins of width 0.4 dex, in addition to one bin of width 0.2 dex at the steep high mass end of the galaxy mass function. We then divided galaxies from the four mass bins into three redshift intervals, spanning a total range of  $0.2 < z < 1.2$ . Galaxies were considered to be central if no other, more massive,

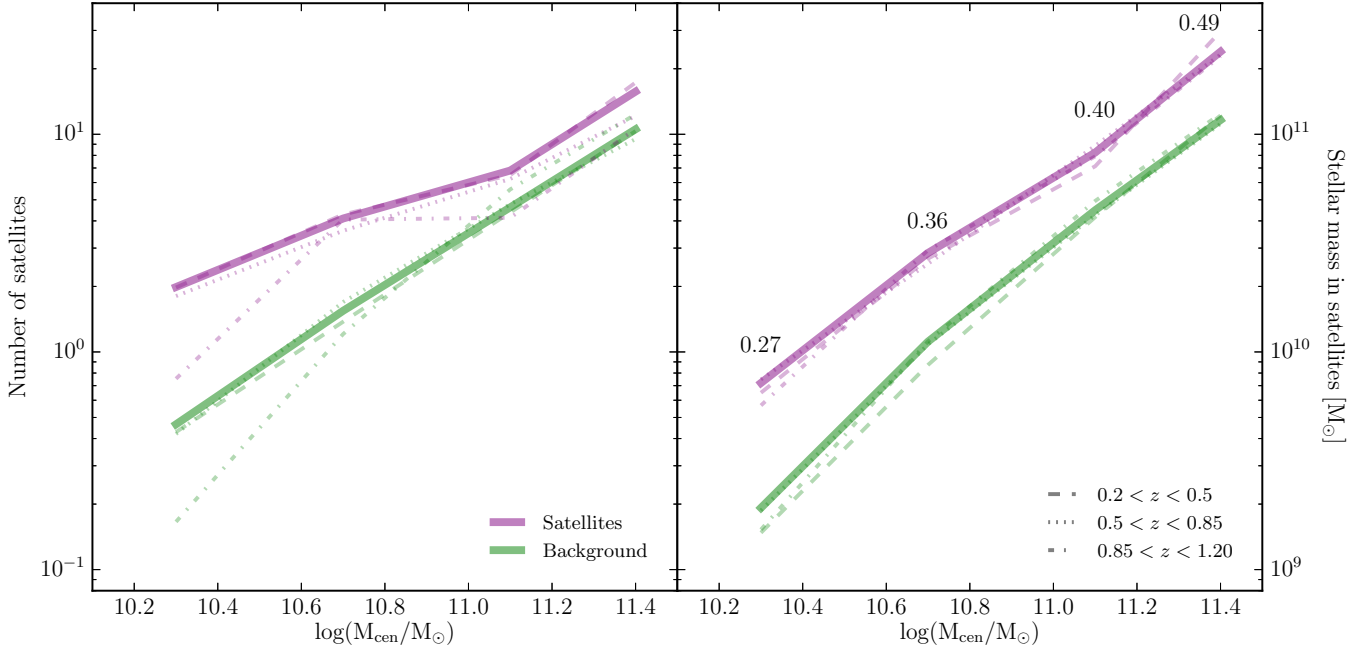


**Figure 2.** Number of satellites and their total stellar mass as a function of central galaxy mass. Solid purple lines represent the number of satellites (left panel) and the total stellar mass enclosed in them (right panel) as estimated by integrating double-Schechter fits to the satellite mass functions at each central mass range (purple line in Figure 1). Dashed, dotted and dot-dashed lines show this calculation at each redshift separately. Green lines depict the same measurements for contaminating background and foreground sources (as extracted from randomly positioned apertures). Broad spectral coverage of photometric data and consequent excellent photometric redshifts in the UltraVISTA catalog allow us to keep a relatively low contaminating source fraction ( $\sim 20\% - 40\%$ ). Also noted in the figure are the average fractional contributions of satellite mass to the overall mass budget in their halos. While satellite galaxies account for only  $\sim 27\%$  of the stellar mass in groups around low mass centrals, satellites around massive centrals contain as much stellar mass as the central galaxy itself.

galaxies could be found within two projected virial radii. Virial radius estimates at a given stellar mass and redshift were determined using the semi-analytic model of Guo et al. (2011).

### 2.2. Statistical Measurement of Satellite Galaxies

In order to study the mass distribution of satellite galaxies around the selected centrals we followed the statistical background subtraction procedure described by Tal et al. (2012b). We utilized photometric redshift measurements from the UltraVISTA catalog to identify all galaxies within two projected virial radii from each central that are separated from it by no more than  $dz = 0.05$ . This choice of aperture size was aimed at making a rather inclusive selection of possible satellite galaxies. While some fraction of these sources are indeed physically associated with the studied groups, other sources are potentially misidentified and instead lie in the background or the foreground of the halo. We account for this contribution of contaminating sources by repeating the same analysis in randomly positioned apertures in the field.

For each central galaxy we selected a position at random from the area allowed by the catalog coverage mask (as described in Muzzin et al. 2013b). At this random position, we identified all galaxies that would be regarded as satellite candidates according to virial radius estimates and redshift of the corresponding central. This procedure was repeated 20 times for each central galaxy.

## 3. SATELLITE GALAXY STELLAR MASS FUNCTIONS

The stellar mass functions of satellite galaxies in the studied groups are revealed after removing the average contribution of contaminating background and fore-

ground sources. We derived the mass distribution of all sources that were found within the central galaxy centered apertures at each redshift in each of the four stellar mass bins. Similarly, we measured the mass functions of sources in randomly positioned apertures, thus quantifying the contribution from galaxies at the same mass and redshift that are not associated with the selected centrals. The difference between the average mass functions in apertures centered around centrals and in apertures centered around randomly selected positions is taken to be the mass distribution of satellite galaxies that are physically associated with the targeted groups. Error estimates in our satellite mass functions include statistical uncertainties as were calculated from the 20 random apertures per central galaxy.

The results are shown in Figure 1. Each panel shows the stellar mass function of satellite galaxies in three redshift intervals over a fixed range of central stellar mass. Completeness limits in stellar mass estimates define the plotted mass range at each redshift. The mass distributions of central galaxies are marked in each panel as black points and a gray region. Solid blue, green and red lines are model fits to each combination of central mass and redshift range, relying on the sum of two Schechter (1976) functions as the underlying model. The thick purple line is a similar double-Schechter model fit to the entire satellite galaxy population in each panel. For comparison, the average mass function from the  $10.1 < \log(M_{\text{cen}}/M_{\odot}) < 10.5$  panel is shown in the other panels as a dashed purple line. Finally, the error bars in Figure 1 mark statistical uncertainties as calculated from the standard deviation of the 20 random mass functions per central galaxy. We note that the choice of double-Schechter model fitting was motivated by re-

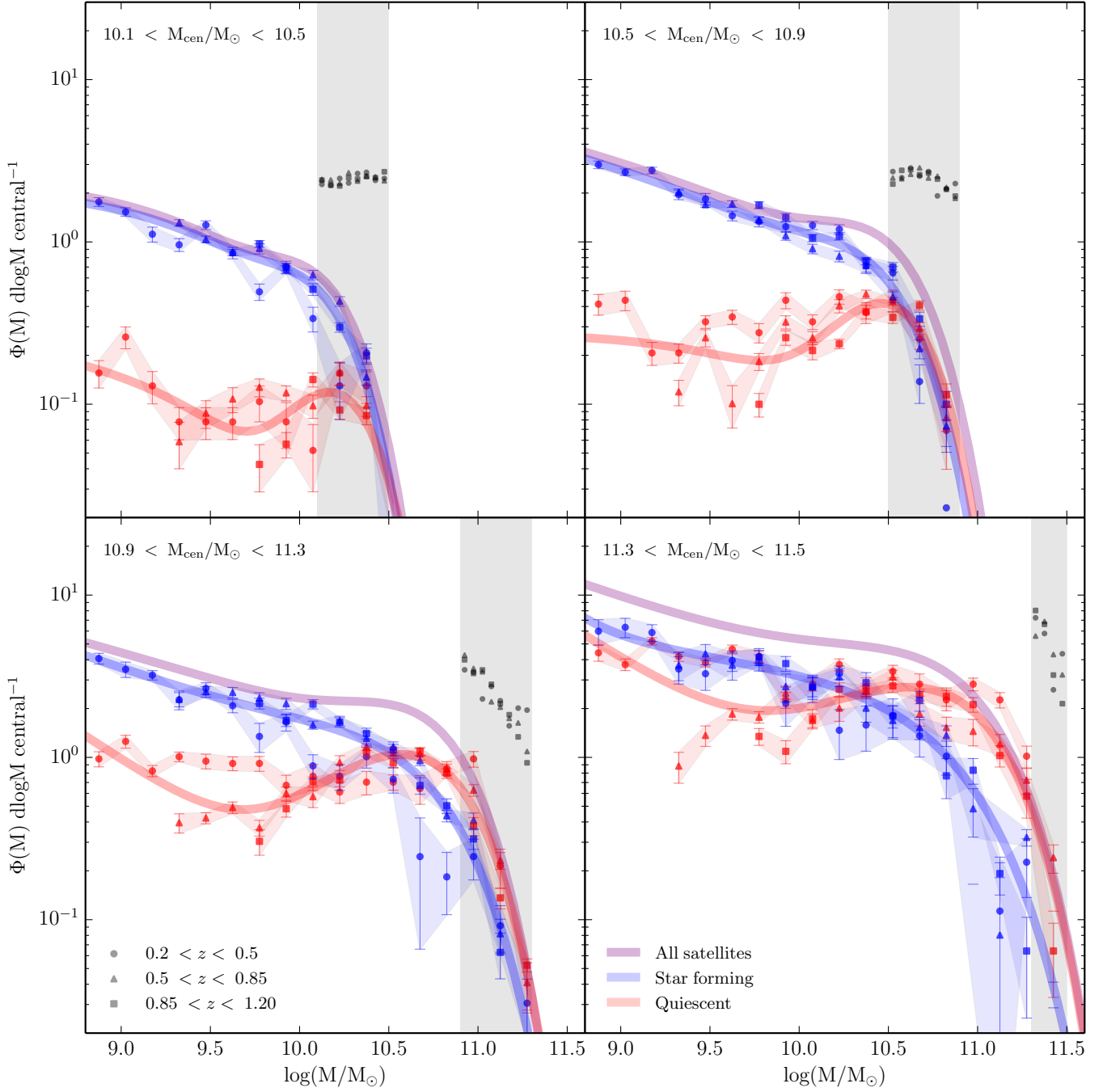


**Figure 3.** Stellar mass function of star forming and quiescent satellite galaxies. Black points and gray regions show the range of central galaxy masses in each panel. Blue and red points represent the mass distribution of star forming and quiescent galaxies, respectively. Different marker symbols denote satellite mass functions at different redshifts. Blue and red lines are double-Schechter fits to the star forming and quiescent satellite data and the thick purple line is a double-Schechter fit to the entire satellite population in each panel (same as in Figure 1). The stellar mass functions of star forming galaxies at different redshifts are consistent with one another in the range  $0.2 < z < 1.2$ , while the mass distributions of quiescent satellites are essentially constant with redshift at  $M_{\text{sat}}/M_{\odot} \gtrsim 10$ . The relative contribution of each subpopulation to the overall satellite mass distribution strongly varies with central mass.

sults from recent studies, who found that such fits better describe galaxy stellar mass functions than a single Schechter function (e.g., Baldry et al. 2008; Li & White 2009; Muzzin et al. 2013a; Tomczak et al. 2014). Best-fit model parameters are given in Table 1.

### 3.1. Lack of Redshift Dependence in the Distribution of Satellite Masses at fixed central mass

The stellar mass functions of satellite galaxies at any of the four central galaxy mass ranges show no sign of sig-

nificant dependence on redshift. As can be seen in Figure 1, satellite mass distributions at different redshifts are consistent with one another within statistical uncertainties. By contrast, the overall distribution of satellite masses is strongly dependent on the mass of their central galaxy (and by proxy also on the group halo mass). This is evident from comparison of the satellite mass function at each selection range of  $M_{\text{cen}}$  with that of the lowest central mass bin (dashed purple curve in Figure 1). The difference between the curves in each of the panels

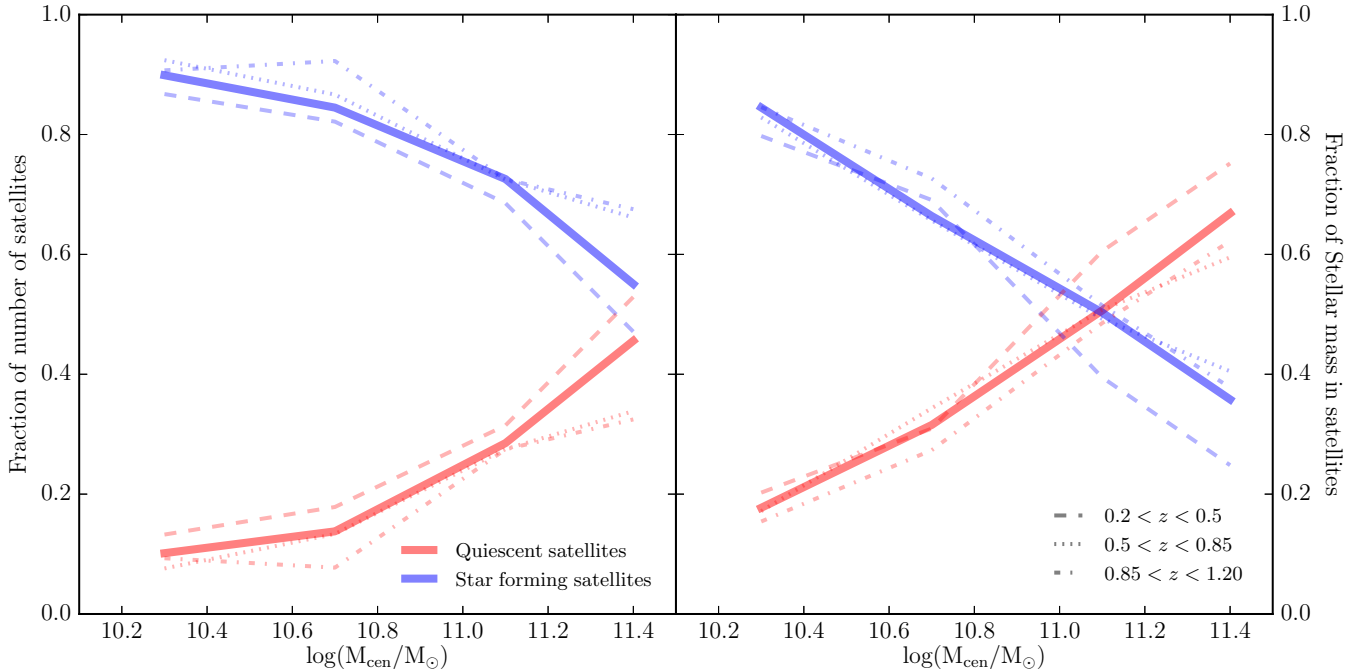


**Figure 4.** Relative contribution of star forming and quiescent satellite galaxies. Blue and red lines show the fractions of satellite counts (left panel) and stellar mass (right panel) of star forming and quiescent satellite galaxies, respectively. The number of quiescent satellites nearly reaches that of star forming satellites at the most massive end of the analyzed central mass range ( $M_{\text{cen}}/M_{\odot} \sim 2.5 \times 10^{11}$ ). However, since quiescent satellites preferentially occupy the massive end of the satellite mass function (as can be seen in Figure 3), the total stellar mass enclosed in them dominates over that of star forming satellites even in lower mass halos (with  $M_{\text{cen}}/M_{\odot} \sim 1.2 \times 10^{11}$ ).

clearly shows that while the slope of the low mass end of the satellite mass function stays relatively unchanged, the overall normalization grows quickly with increasing central mass.

The strong dependence of the stellar mass function of satellite galaxies on the mass of their central galaxy at  $z = 0$  has been demonstrated by Yang et al. (2009). Here we show that this dependence holds to at least  $z = 1.2$ . Remarkably, this suggests that the mass distribution of satellite galaxies can essentially be characterized by a single parameter (either central galaxy mass or its associated halo mass) over more than 60% of the age of the universe. The simplicity of this observed relation is accentuated by the complexity of processes that determine the distribution of satellite masses in individual groups. Strikingly, the combined effect of such processes apparently does not depend on redshift in the range  $0.2 < z < 1.2$ .

### 3.2. Contribution of Satellites to the Group Stellar Mass Budget

Figure 2 shows the overall growth in the number and mass of satellite galaxies with increasing central galaxy mass (purple lines). The total number density (left panel) and stellar mass density (right panel) of satellite galaxies were derived by integrating each best-fit model from Figure 1 over the satellite mass range  $8.7 < \log(M/M_{\odot}) < 12.0$ . For comparison, we also show the total number and mass of contaminating sources as derived from randomly positioned apertures (green lines). The number and mass of satellite galaxies grow dramatically over the studied central mass range. Around the lowest mass centrals we find an average number of 2 satellites which make up roughly 27% of the total stellar mass in the group. Around the most massive centrals this

number increases to nearly 16 satellites, and the total stellar mass that is enclosed in them roughly equals the stellar mass of their centrals. As groups undergo hierarchical growth at  $z < 1$  (e.g., Williams et al. 2012), they move up the track in Figure 1. This result suggests that the stellar mass in central and satellite galaxies must grow in tandem, and that the total mass in satellites grows at a faster rate than that of centrals.

## 4. STELLAR MASS FUNCTIONS OF QUIESCENT AND STAR FORMING SATELLITES

In this section we analyze the mass distributions of star forming and quiescent satellites separately. We do so by classifying each galaxy in our sample as either “star forming” or “quiescent”, following the method described by Williams et al. (2009) and later successfully repeated in numerous studies (e.g., Brammer et al. 2011; Szomoru et al. 2012; Barro et al. 2013; Muzzin et al. 2013a; Tal et al. 2014). Williams et al. (2009) showed that galaxies out to  $z = 2$  can be reliably identified as having a low star formation rate based on a set of rest frame  $U - V$  vs.  $V - J$  ( $UVJ$ ) color selection criteria. Here we adopt the  $UVJ$  threshold values that were found by Muzzin et al. (2013b) using redshift and rest frame color estimates from the same UltraVISTA survey catalog that we utilize in this study.

Figure 3 shows the resulting stellar mass functions of star forming and quiescent satellites as a function of central galaxy mass and redshift. As in Figure 1, black points mark central galaxy masses and thick purple lines follow the best-fit double-Schechter model to the entire sample in a given panel. Blue and red points and error bars show the mass distributions and statistical uncertainties of star forming and quiescent galaxies, respectively. Thick blue and red lines depict the best double-



**Table 1**  
Double-Schechter best fit parameters

All galaxies					
Central mass	$\log(M^*/M_\odot)$	$\alpha_1$	$\log(\Phi_1^*)$	$\alpha_2$	$\log(\Phi_2^*)$
$10.1 < M_{\text{cen}} < 10.5$	$9.61 \pm 0.01$	$1.55 \pm 0.52$	$0.29 \pm 0.04$	$-1.05 \pm 0.05$	$0.87 \pm 0.08$
$10.5 < M_{\text{cen}} < 10.9$	$10.09 \pm 0.01$	$0.83 \pm 0.13$	$0.91 \pm 0.04$	$-1.28 \pm 0.01$	$0.71 \pm 0.03$
$10.9 < M_{\text{cen}} < 11.3$	$10.41 \pm 0.01$	$-1.29 \pm 0.01$	$0.77 \pm 0.07$	$0.42 \pm 0.10$	$1.81 \pm 0.10$
$11.3 < M_{\text{cen}} < 11.5$	$10.73 \pm 0.01$	$-1.40 \pm 0.06$	$0.85 \pm 0.76$	$-0.31 \pm 0.21$	$3.67 \pm 0.47$
Star forming					
Central mass	$\log(M^*/M_\odot)$	$\alpha_1$	$\log(\Phi_1^*)$	$\alpha_2$	$\log(\Phi_2^*)$
$10.1 < M_{\text{cen}} < 10.5$	$9.60 \pm 0.01$	$1.44 \pm 0.64$	$0.27 \pm 0.04$	$-1.04 \pm 0.06$	$0.81 \pm 0.08$
$10.5 < M_{\text{cen}} < 10.9$	$10.07 \pm 0.01$	$0.56 \pm 0.27$	$0.69 \pm 0.03$	$-1.30 \pm 0.02$	$0.62 \pm 0.05$
$10.9 < M_{\text{cen}} < 11.3$	$10.53 \pm 0.02$	$-0.46 \pm 0.67$	$0.85 \pm 0.13$	$-1.42 \pm 0.12$	$0.34 \pm 0.28$
$11.3 < M_{\text{cen}} < 11.5$	$10.81 \pm 0.01$	$-1.13 \pm 0.02$	$1.26 \pm 0.11$	$-2.91 \pm 30.6$	$0.01 \pm 0.01$
Quiescent					
Central mass	$\log(M^*/M_\odot)$	$\alpha_1$	$\log(\Phi_1^*)$	$\alpha_2$	$\log(\Phi_2^*)$
$10.1 < M_{\text{cen}} < 10.5$	$9.63 \pm 0.01$	$2.53 \pm 0.96$	$0.02 \pm 0.01$	$-1.17 \pm 0.14$	$0.06 \pm 0.01$
$10.5 < M_{\text{cen}} < 10.9$	$10.00 \pm 0.01$	$1.96 \pm 0.55$	$0.14 \pm 0.01$	$-1.00 \pm 0.11$	$0.12 \pm 0.01$
$10.9 < M_{\text{cen}} < 11.3$	$10.46 \pm 0.01$	$0.33 \pm 0.04$	$1.15 \pm 0.01$	$-1.72 \pm 0.06$	$0.04 \pm 0.01$
$11.3 < M_{\text{cen}} < 11.5$	$10.71 \pm 0.01$	$-1.71 \pm 0.14$	$0.11 \pm 0.03$	$-0.12 \pm 0.14$	$3.03 \pm 0.16$

<sup>a</sup>The single Schechter model is defined as:  $\Phi(M) = \ln(10)\Phi^* \left[ 10^{(M-M^*)(1+\alpha)} \right] \times \exp \left[ 10^{(M-M^*)} \right]$

Schechter model fits to all galaxies in their respective subpopulation.

#### 4.1. Rise of the Massive Quiescent Satellites

Similarly to the overall satellite mass functions, the mass distributions of both star forming and quiescent satellites exhibit no more than a weak dependence on redshift. The stellar mass functions of star forming satellite galaxies at any given central mass are consistent with one another over the entire analyzed redshift range (blue lines in Figure 3). The same appears to be true for quiescent satellites at high masses ( $\log(M/M_\odot) \gtrsim 10$ ), although there is possible evidence for growth with time at lower masses (with large uncertainties). We note that evidence for different evolution at the low and high end of the mass spectrum of quiescent galaxy populations has also been found in studies of the global stellar mass function (e.g., Peng et al. 2010; Moustakas et al. 2013; Muzzin et al. 2013a; Tomczak et al. 2014).

The main difference between the mass functions of star forming and quiescent galaxies is in their relative contribution to the overall satellite mass distribution as a function of central mass. While the fraction of star forming galaxies at all satellite mass bins decreases with increasing central mass, the fraction of quiescent satellites rises sharply. Moreover, the relative number of galaxies from each subpopulation does not vary evenly across the satellite mass range. Quiescent satellites preferentially occupy the high mass end of the stellar mass function (at  $\log(M/M_\odot) \gtrsim 10$ ) and make up most of the massive satellite population around massive centrals. At the same time, star forming galaxies account for most of the low mass satellites in all analyzed central galaxy mass bins.

This can be seen in Figure 4, where we calculate the fractional contribution of star forming and quiescent galaxies to the overall number density (top left) and mass density (top right) of satellites as a function of central mass. As before, solid blue and red lines represent star forming and quiescent galaxy subpopulations

over  $0.2 < z < 1.2$ , and dashed, dotted and dot-dashed lines show similar measurements at individual redshift bins. While star forming satellites make up the majority of the satellite galaxy population around centrals in all mass bins, the total mass in quiescent galaxies dominates the mass budget around massive centrals, at  $\log(M/M_{\text{cen}}) \gtrsim 11.1$ .

## 5. SUMMARY

The stellar mass function of satellite galaxies is an important ingredient in galaxy evolution studies, as its shape and normalization are strongly affected by several key processes in group and cluster halos. In this letter we utilized statistical background subtraction to derive satellite mass functions in three fixed stellar mass samples of central galaxies in the redshift range  $0.2 < z < 1.2$ .

We showed that the mass distribution of satellite galaxies is independent of redshift for any given value of central galaxy mass. In addition, since the satellite mass function increases strongly with the mass of the central, this suggests that as groups grow with time, they move along a universal central-to-total stellar mass relation.

In addition, we integrated the mass functions of all samples and showed that on average, the number of satellites increases from roughly 2 around central galaxies at  $\log(M_{\text{cen}}/M_\star) \sim 10.3$  to more than 16 at  $\log(M_{\text{cen}}/M_\star) \sim 11.4$ . Furthermore, the total stellar mass that is enclosed in satellite galaxies increases from roughly 27% of the total group mass at the low mass end to nearly 50%, where the most massive centrals in this study contain as much stellar mass as their satellites.

Finally, we derived stellar mass functions for star forming and quiescent satellites independently, and found that both are at most weakly dependent on redshift at fixed central mass. We showed that the relative contribution of each subpopulation to the overall number and mass of satellites varies with central mass and that quiescent satellites preferentially occupy the high mass end of the mass spectrum. As a result, the fraction of quiescent

satellites reaches  $\sim 46\%$  around the most massive subset of analyzed centrals ( $M_{\text{cen}}/M_{\odot} \sim 11.4$ ), where more than 65% of the total satellite mass is locked in quiescent galaxies.

This is the first time that such an analysis is performed at the stellar mass and redshift ranges that are presented here, and it demonstrates that despite the complexity and large range of processes that govern satellite galaxy evolution, the resulting average satellite mass function follows a simple relation with central mass out to  $z \sim 1.2$ .

We thank Kim-Vy Tran for engaging discussions which contributed to this work.

TT is supported by an NSF Astronomy and Astrophysics Postdoctoral Fellowship under award AST-1202667.

This study is based in part on a  $K_s$ -selected catalog of the COSMOS/UltraVISTA field from Muzzin et al. (2013b). The catalog contains PSF-matched photometry in 30 photometric bands covering the wavelength range  $0.15\mu\text{m} \rightarrow 24\mu\text{m}$  and includes the available *GALEX* (Martin et al. 2005), CFHT/Subaru (Capak et al. 2007), UltraVISTA (McCracken et al. 2012), S-COSMOS (Sanders et al. 2007), and zCOSMOS (Lilly et al. 2009) datasets. The catalog was derived using data products from observations made with ESO telescopes at the La Silla Paranal Observatory under ESO programme ID 179.A-2005 and on data products produced by TERAPIX and the Cambridge Astronomy Survey Unit on behalf of the UltraVISTA consortium.

## REFERENCES

- Baldry, I. K., Glazebrook, K., & Driver, S. P. 2008, *MNRAS*, **388**, 945
- Barro, G., Faber, S. M., Pérez-González, P. G., et al. 2013, *ApJ*, **765**, 104
- Bell, E. F., McIntosh, D. H., Katz, N., & Weinberg, M. D. 2003, *ApJS*, **149**, 289
- Bolzonella, M., Kova, K., Pozzetti, L., et al. 2010, *A&A*, **524**, 76
- Brammer, G. B., Whitaker, K. E., van Dokkum, P. G., et al. 2011, *ApJ*, **739**, 24
- Budzynski, J. M., Koposov, S. E., McCarthy, I. G., McGee, S. L., & Belokurov, V. 2012, *MNRAS*, **423**, 104
- Bundy, K., Ellis, R. S., Conselice, C. J., et al. 2006, *ApJ*, **651**, 120
- Capak, P., Aussel, H., Ajiki, M., et al. 2007, *ApJS*, **172**, 99
- Croton, D. J., Springel, V., White, S. D. M., et al. 2006, *MNRAS*, **365**, 11
- Deason, A. J., Conroy, C., Wetzel, A. R., & Tinker, J. L. 2013, *ApJ*, **777**, 154
- Guo, Q., White, S., Boylan-Kolchin, M., et al. 2011, *MNRAS*, **413**, 101
- Ilbert, O., Salvato, M., Le Floc'h, E., et al. 2010, *ApJ*, **709**, 644
- Jones, L. R., Ponman, T. J., Horton, A., et al. 2003, *MNRAS*, **343**, 627
- Knobel, C., Lilly, S. J., Kova, K., et al. 2013, *ApJ*, **769**, 24
- Kovač, K., Lilly, S. J., Knobel, C., et al. 2010, *ApJ*, **718**, 86
- Kroupa, P. 2001, *MNRAS*, **322**, 231
- Li, C., & White, S. D. M. 2009, *MNRAS*, **398**, 2177
- Lilly, S. J., Le Brun, V., Maier, C., et al. 2009, *ApJS*, **184**, 218
- Marchesini, D., van Dokkum, P. G., Förster Schreiber, N. M., et al. 2009, *ApJ*, **701**, 1765
- Martin, D. C., Fanson, J., Schiminovich, D., et al. 2005, *ApJL*, **619**, L1
- Masjedi, M., Hogg, D. W., & Blanton, M. R. 2008, *ApJ*, **679**, 260
- Masjedi, M., Hogg, D. W., Cool, R. J., et al. 2006, *ApJ*, **644**, 54
- McCracken, H. J., Milvang-Jensen, B., Dunlop, J., et al. 2012, *A&A*, **544**, 156
- Milosavljević, M., Miller, C. J., Furlanetto, S. R., & Cooray, A. 2006, *ApJL*, **637**, L9
- Moustakas, J., Coil, A. L., Aird, J., et al. 2013, *ApJ*, **767**, 50
- Muzzin, A., Marchesini, D., Stefanon, M., et al. 2013a, *ArXiv e-prints*, 1303.4409
- . 2013b, *ApJS*, **206**, 8
- Nierenberg, A. M., Auger, M. W., Treu, T., et al. 2012, *ApJ*, **752**, 99
- Peng, Y.-j., Lilly, S. J., Kova, K., et al. 2010, *ApJ*, **721**, 193
- Sanders, D. B., Salvato, M., Aussel, H., et al. 2007, *ApJS*, **172**, 86
- Schechter, P. 1976, *ApJ*, **203**, 297
- Szomoru, D., Franx, M., & van Dokkum, P. G. 2012, *ApJ*, **749**, 121
- Tal, T., & van Dokkum, P. G. 2011, *ApJ*, **731**, 89
- Tal, T., van Dokkum, P. G., Franx, M., et al. 2013, *ApJ*, **769**, 31
- Tal, T., Wake, D. A., & van Dokkum, P. G. 2012a, *ApJL*, **751**, L5
- Tal, T., Wake, D. A., van Dokkum, P. G., et al. 2012b, *ApJ*, **746**, 138
- Tal, T., Dekel, A., Oesch, P., et al. 2014, *ArXiv e-prints*, 1401.2984
- Tomczak, A. R., Quadri, R. F., Tran, K.-V. H., et al. 2014, *ApJ*, **783**, 85
- van den Bosch, F. C., Yang, X., Mo, H. J., et al. 2007, *MNRAS*, **376**, 841
- van der Burg, R. F. J., Muzzin, A., Hoekstra, H., et al. 2013, *A&A*, **557**, 15
- Vulcani, B., Poggianti, B. M., Oemler, A., et al. 2013, *A&A*, **550**, 58
- Wang, W., & White, S. D. M. 2012, *MNRAS*, **424**, 2574
- Williams, R. J., Kelson, D. D., Mulchaey, J. S., et al. 2012, *ApJL*, **749**, L12
- Williams, R. J., Quadri, R. F., Franx, M., van Dokkum, P., & Labbé, I. 2009, *ApJ*, **691**, 1879
- Yang, X., Mo, H. J., & van den Bosch, F. C. 2008, *ApJ*, **676**, 248
- . 2009, *ApJ*, **695**, 900
- Yang, X., Mo, H. J., van den Bosch, F. C., et al. 2007, *ApJ*, **671**, 153